Journal of Alloys and Compounds 504 (2010) 7–11

Contents lists available at ScienceDirect

Journal of Alloys and Compounds

journal homepage: www.elsevier.com/locate/jallcom

Structural, electrical and optical properties of $Cd_{1-x}Gd_xO$ nanocomposite thin films

A.A. Dakhel

Department of Physics, College of Science, University of Bahrain, P.O. Box 32038, Bahrain

ARTICLE INFO

Article history:
Received 10 February 2010
Received in revised form 9 May 2010
Accepted 13 May 2010
Available online 27 May 2010

PACS:
78.20.Ci
72.20.−i
78.70.En

Keywords:
Optical properties
Cadmium–gadolinium oxide
Gd-doped CdO
Mobility
Oxides
Degenerate semiconductors
Rare earth oxides
TCO

ABSTRACT

Gd-doped CdO thin films with various Gd compositions were prepared on glass and Si wafer substrates using a vacuum evaporation technique. The influence of varying Gd composition on structural, electrical, and optical properties of the prepared films were systematically investigated. Experimental data indicate that Gd^{3+} doping slightly stress the CdO crystalline structure and change its optoelectronic properties. The bandgap of Gd-doped CdO suffers narrowing by about 40% due to a small (0.2%) doping level. The electrical behaviours of the Gd-doped CdO films show that they are degenerate semiconductors. The 0.6% Gd-doped CdO film shows increase its mobility by about eight times, conductivity by 150 times, and carrier concentration by 20 times, relative to undoped CdO film. However, the largest mobility of 66.7 $cm^2/V\,s$ was obtained for 0.2% Gd-doped CdO film. From transparent-conducting-oxide point of view, the Gd is effectively suitable for CdO doping. Finally, the absorption in the NIR spectral region was studied in the framework of the classical Drude theory.

1. Introduction

Cadmium oxide CdO is one of degenerate semiconductors that has a wide range of applications in optoelectronics like transparent conducting oxide (TCO), solar cells, smart windows, optical communications, flat panel display, photo-transistors, as well as other type of applications like IR heat mirror, gas sensors, low-emissive windows, and thin-film resistors, etc. [1,2–5]. These applications are based on its electrical and optical properties. From electrical side, nonstoichiometric CdO has n-type semiconducting behaviour with relatively low electrical resistivity (10^{-2}–$10^{-4}\ \Omega$ cm) due to its native defects of oxygen vacancies and cadmium interstitials. From optical side, it is transparent in visible and NIR spectral regions with a direct bandgap of 2.2–2.7 eV [1,6–9]. It crystallises in a cubic structure of Fm3m space group of 6-coordination [10]. The opto-electrical properties of CdO could be controlled by doping with different metallic ions like In, Sn, Al, Sc, Y, Tl, etc., which improves its electrical conduction and increases its optical bandgap following Moss–Burstein (B–M) effect [1,5,11–16]. It is possible to dope CdO with magnetic ions like Fe [17] in order to combine some magnetic properties with its optoelectronic properties for different applications. In addition, it is possible to dope with rare-earth 4f-ions like Sm or Dy [18,19]. The present work report the electrical and optical properties of Gd-doped CdO with different doping levels. As expected, when Gd^{3+} ions substitute some Cd^{2+} ions in CdO crystalline structure, the concentration of conduction electrons should be increased that is finally leads to improve the electrical conduction. It was observed that when the dopant ions have radius less than that of Cd^{2+} then the conductivity of the doped CdO increases and the lattice unit cell compresses, while the addition of ions with an ionic radii equal or greater than Cd^{2+}, does not significantly alter the lattice parameters. In the present case the 6-coordination ionic radius of Gd^{3+} is 0.0938 nm, which is slightly smaller than that of Cd^{2+} ion, 0.0947 nm [20]. It must be mentioned that, the doping of CdO with Gd ions by any technique, to our best knowledge, is absent from the literature.

2. Experimental

The $Cd_{1-x}Gd_xO$ thin films of various compositions were grown on glass and silicon substrates. The detailed deposition procedure have been described elsewhere [18,19]. The as-grown films were partially oxidised. They were oxidised and stabilised by annealing in air at 400 °C for 2 h. All samples were prepared in almost

E-mail address: adakhil@sci.uob.bh.

0925-8388/$ – see front matter © 2010 Elsevier B.V. All rights reserved.
doi:10.1016/j.jallcom.2010.05.063

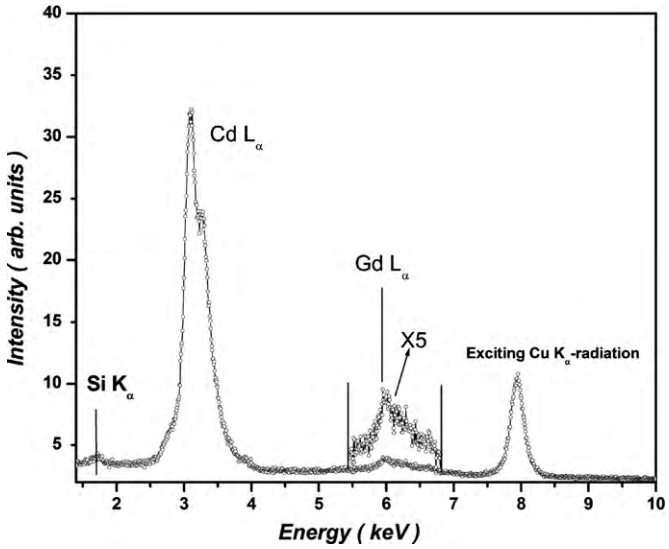

Fig. 1. X-ray fluorescence of Gd-doped CdO film grown on Si substrate. The exciting radiation was Cu K_α.

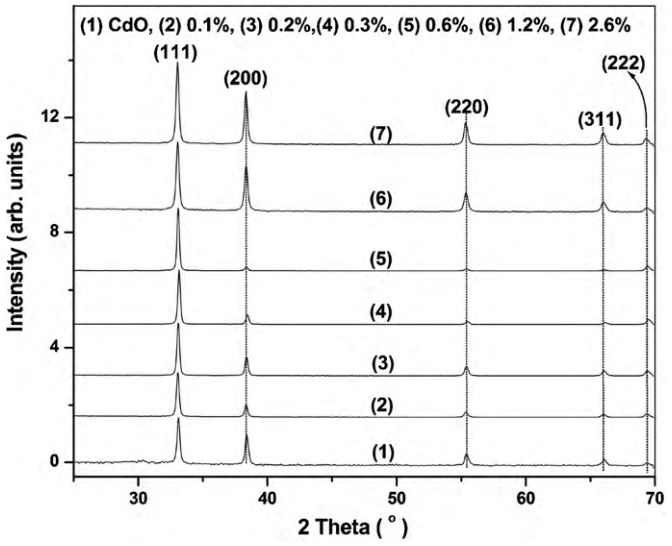

Fig. 2. X-ray diffraction patterns from undoped and Gd-doped CdO films prepared at different Gd dopant % levels. The used radiation was Cu K_α-line.

the same conditions including the reference undoped CdO film. The evaporated masses were controlled with a Philips FTM 5 thickness monitor and measured after annealing by an MP100-M spectrometer (Mission Peak Optics Inc., USA) to be in the range of 0.15–0.25 μm. The structure of the prepared films was studied by the X-ray diffraction (XRD) method using a Philips PW 1710 θ–2θ system with Cu K_α radiation (0.15406 nm) and a step size of 0.02°. The energy dispersion X-ray fluorescence (EDX) method was used to determine the relative weight ratio Gd to Cd(r) in the studied samples to be about 0.1 wt%, 0.2 wt%, 0.3 wt%, 0.6 wt%, 1.2 wt%, and 2.6 wt%. The spectral optical transmittance $T(\lambda)$ and reflectance $R(\lambda)$ were measured at normal incidence in UV–Vis–NIR spectral region (500–3000 nm) with a Shimadzu UV-3600 double beam spectrophotometer. The electrical measurements were carried out with a standard Van-der-Pauw method with aluminum dot contacts in a magnetic field of about 1 T and using a Keithley 195A digital multimeter and a Keithley 225 current source.

3. Results and discussion

3.1. Characterisation by X-rays

Fig. 1 demonstrates the energy-dispersive X-ray fluorescence (EDX) spectrum of the prepared thin Gd-doped CdO film on silicon substrate. The spectrum shows the Cd L-spectrum (3.13–3.53 keV) and Gd L-spectrum (6.05–7.1 keV) with some signals from the source and silicon substrate. The ratio of integral intensity of Gd L-signal, I_{Gd} to that of Cd L-signal, I_{Cd} or (I_{Gd}/I_{Cd}) was used to determine the relative weight fraction ratio of Gd to Cd in a film sample. For that purpose, the known method of micro-radiographic analysis was used [21]. The reference samples were pure Gd_2O_3 and CdO thin films. The results are given in Table 1.

Fig. 2 shows the X-ray diffraction (XRD) patterns of the prepared undoped and Gd-doped CdO films. The patterns reveal that all the investigated films are polycrystalline of cubic Fm3m CdO structure [10]. The usually energetically favourable (1 1 1) preferred orientation growth of CdO films, prepared by different techniques [22–25], is studied here through the texture coefficient (TC). It is defined [26] as, $TC(h\,k\,l) = [nI_r(h\,k\,l)/I_{std}(h\,k\,l)]/[\sum_{k=1}^{n} I_r^k(h\,k\,l)/I_{std}^k(h\,k\,l)]$, where $I_r(h\,k\,l)$ is the relative intensity of reflection from a given $(h\,k\,l)$ plane, $I_{stn}(h\,k\,l)$ is the relative intensity of the reflection from the same plane as indicated in a standard sample (Ref. [10]), and n is the total number of reflections observed, which is five in the present investigation. The calculated values of TC are given in Table 1. The mean X-ray grain size (GS) perpendicular to [1 1 1] direction was estimated by using Scherrer's relation [27]. The results are also given in Table 1. The inset of Fig. 3 shows the variation of GS and TC with Gd% content in the CdO films, where one can observe identical trends. However, the largest values for GS and TC are observed for 0.6% Gd film. It is also observed that there are a slight shift $\Delta(2\theta_{111})$ in the position of the intense CdO(1 1 1) reflection towards higher Bragg angle, relative to that for the source CdO powder, 33.04° (Table 1 and Fig. 3). The Bragg position $2\theta_{111}$ for the prepared undoped CdO film is also shifted towards higher angle due to the formation of the structural vacancies (nonstoichiometric composition) that cause electrical conduction in the film. Due to the

Table 1
The Bragg angle $(2\theta^{\circ}_{(111)})$, the average X-ray grain size perpendicular to [1 1 1] direction (GS), and the texture coefficient [TC(1 1 1)] for the prepared undoped and Gd-doped CdO films on glass substrates.

Sample	$2\theta^{\circ}_{(111)}$	GS (nm)	TC(1 1 1)
Powder	33.04	–	–
CdO	33.11	34.7	1.54
0.1%	33.07	35.2	2.08
0.2%	33.12	38.3	1.80
0.3%	33.18	37.1	2.32
0.6%	33.11	41.7	2.76
1.2%	33.07	31.8	1.47
2.6%	33.06	30.9	1.48

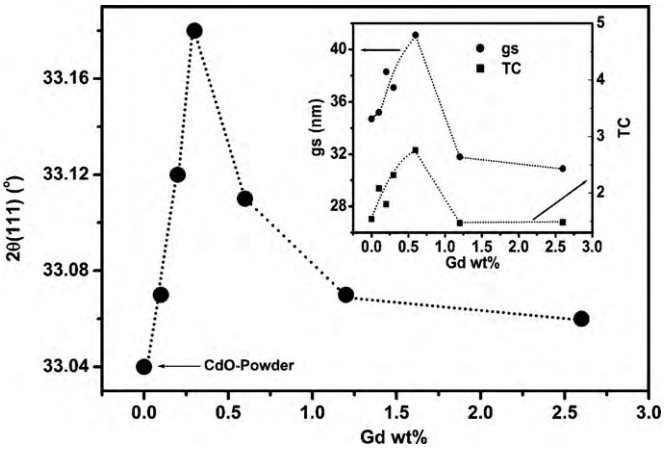

Fig. 3. Variation of Bragg angle 2θ for CdO(1 1 1) reflection with the Gd% doping level. The inset shows the variation of X-ray grain size (GS) and texture coefficient (TC) with the Gd% doping level.

Table 2
Summary of the measured electrical parameters (resistivity, ρ, mobility, μ_{el}, and carrier concentration, N_{el}) and bandgap, E_g for undoped and Gd-doped CdO films on glass substrates. The ratio (N/μ) measured optically (Op) and electrically (el) are given in units ($\times 10^{28}$ V s/m^5).

Sample	ρ ($\times 10^{-4}$ Ω cm)	μ_{el} (cm^2/V s)	N_{el} ($\times 10^{20}$ cm^{-3})	E_g (eV)	$(N/\mu)_{el}$	$(N/\mu)_{Op}$
CdO	201	7.03	0.44	2.4	6.28	3.44
0.1%	12.30	27.6	1.83	1.9	6.63	4.86
0.2%	3.05	66.7	3.05	1.4	4.57	21.3
0.3%	1.84	62.5	5.40	2.1	8.65	31.56
0.6%	1.30	55.7	8.66	2.0	15.5	34.2
1.2%	8.1	17.1	4.51	1.9	25.0	24.95
2.6%	8.46	18.6	3.95	2.4	21.23	17.43

slightly smaller size of Gd^{3+} relative to that of Cd^{2+} ion, the doping creates structural strain, that causes the (1 1 1) reflection of Gd-doped CdO films to shift to higher angles relative to that of the CdO powder. The created structural strain by Gd^{3+} ion doping can be estimated by using $\varepsilon_s = -\Delta\theta_{(111)} \cot \theta_{(111)}$, which is of order -10^{-3}, i.e. a slight decrease of lattice parameter of order 0.1%. Fig. 3 shows the variation of $2\theta_{111}$ with Gd^{3+} doping level. The behaviour of the dependence shows the limited solubility of Gd in CdO.

3.2. DC-electrical properties

The room temperature electrical resistivity (ρ), mobility (μ_{el}), and carrier concentration (N_{el}) were measured by a standard Vander-Pauw method and the results are presented in Table 2 and Fig. 4. The main source of experimental error is being due to the sample size and circular-aluminum contact spot size, which was estimated to be about 5%. The electrical measurements show that the undoped and all Gd-doped CdO samples are n-type semiconductors. The measured electrical parameters (ρ, N_{el}, and μ_{el}) of undoped CdO film agree with those data published for CdO films prepared by different techniques [1,28–32]. However, the measured resistivity of the undoped CdO film in the present work, is larger than those values mentioned in some other references $\sim 10^{-3}$–10^{-4} Ω cm due to different method and procedure of preparation. The present results show that doping of CdO with Gd ions changes all the electrical parameters. For all studied Gd concentration doping, the conductivity σ, carrier concentration, and the mobility increase relative to undoped CdO film. The carrier concentration N_{el} and conductivity get maximum values for 0.6% Gd sample. The mobility, as a resultant of both the resistivity and carrier concentration $\mu_{el} = (e\rho N_{el})^{-1}$, gets largest value for 0.2–0.3% Gd films. These changes are resulted from the variation in the carrier concentration, carrier scattering (by microstructural defects, grain boundaries, and ionised impurities) and intrinsic bandgap (this will be discussed later). Doping with Gd ions includes substitution of Cd^{2+} ions with Gd^{3+} ions, which liberates more conduction electrons in the conduction band. Thus, Gd dopant plays principally the same role as other usual metallic dopants like In, Sn, Al, Sc, and Y. In a summary, the present work proves that low doping with Gd improves the dc-conduction parameters of CdO, so that the 0.6% Gd-doped CdO film shows an increase in its mobility by about eight times, conductivity by 150 times, and carrier concentration by 20 times, relative to undoped CdO film. Fig. 4 demonstrates that for lower Gd% doping levels, N_{el}, σ, and μ_{el} increase. However, when the Gd% content increases as in samples 1.2% and 2.6%, the situation changes so that the all electrical parameters (N_{el}, σ, and μ_{el}) decreased. This can be explained by gradual arising of another factor namely the Gd accumulation on the grain boundaries (GB), which increase the GB scattering that reduces μ_{el}, σ, and the effective carrier concentration participates in the dc-conduction process. Fig. 4 shows that the utmost change in all electrical parameters is observed for 0.3–0.6% samples and in the lattice parameter is observed for 0.3% sample; these changes are induced by Gd doping in CdO. Thus, one can deduce that the solubility of Gd in CdO is very limited and may be of order ~0.3%.

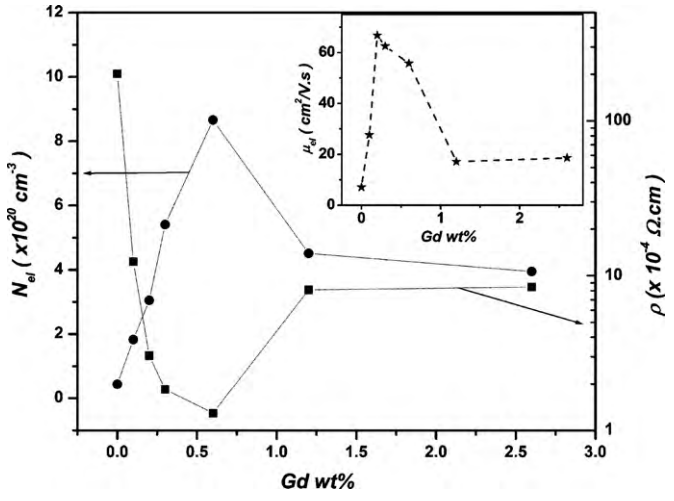

Fig. 4. Variation of resistivity, mobility, and carrier concentration for undoped and Gd-doped CdO films prepared on glass substrates at different Gd dopant % levels.

3.3. Optoelectronic properties

The spectral optical absorption measurements are used to study the optical properties of the prepared Gd-doped CdO films grown on corning glass substrates. The experimentally corrected normal spectral transmittance $T(\lambda)$ in the UV–Vis–NIR region (500–3000 nm) are presented in Fig. 5a and b. Any special absorption peak or feature in the wavelength range studied that is related to 4f electrons (like 4f–5d transition) was not observed. The spectra show that the maxima of the spectral transmittance for all investigated films are being in the NIR region. In addition, at NIR region, the transmittance curves show a clear damping, especially for Gd-doped CdO samples due to high density of the free electrons. The normal reflectance from all the samples studied in UV, Vis, and NIR is almost constant and close to each other in magnitude of 1–3%. The spectral absorption coefficient $\alpha(\lambda)$ is calculated from the experimental data by using the following equation [33,34]: $\alpha(\lambda) = (1/d)\ln[(1-R)/T]$, where d is the film thickness. The optical direct bandgap E_g is evaluated according to the well-known energy-exponential relation [35,36]:

$$\alpha E = A_{Op}(E - E_g)^m \quad (1)$$

where A_{Op} is a constant and the exponent m is equal to 0.5 or 2 for direct and indirect transitions, respectively. Thus, the plot of $(\alpha E)^2$ vs. E as shown in Fig. 6 gives the value of direct bandgap (with estimated error ±0.1 eV). The obtained bandgaps for undoped and Gd-doped CdO films are given in Table 2. For undoped CdO, the bandgap obtained is in the range (2.2–2.6 eV) that known for undoped CdO films prepared by different techniques [1,37,38]. It is observed that the bandgaps of Gd-doped CdO films are narrower than that of undoped CdO film. For example, doping of CdO with

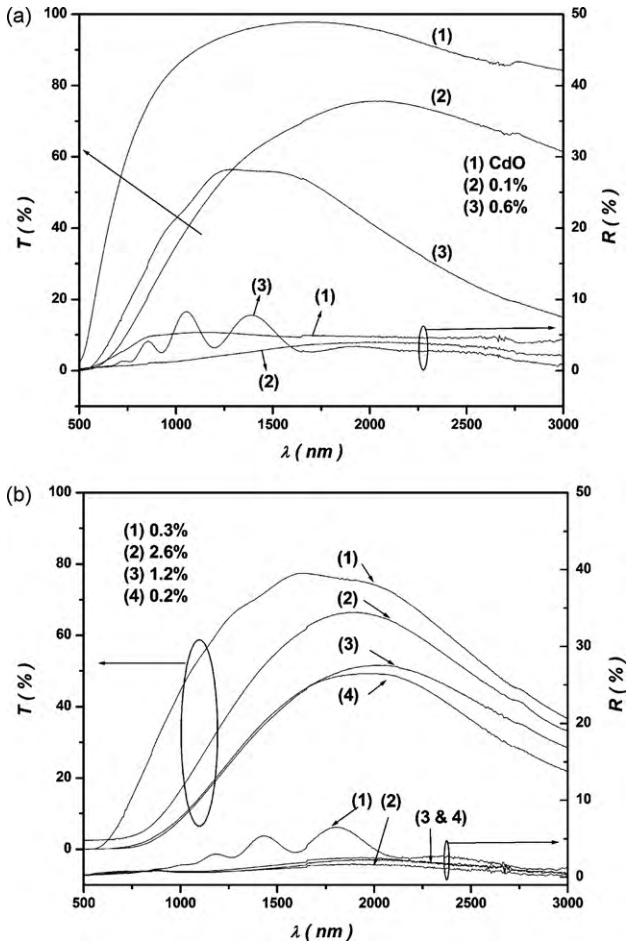

Fig. 5. Spectral normal transmittance and reflectance in the UV–Vis–NIR spectral regions for undoped and Gd-doped CdO films prepared on glass substrates at different Gd dopant % levels.

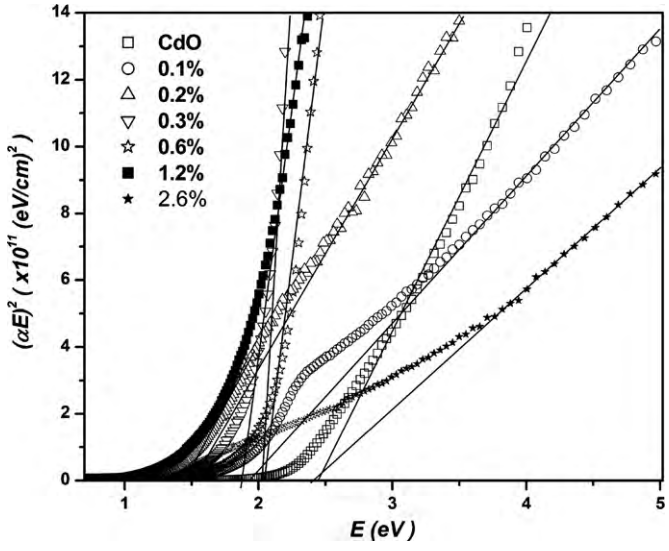

Fig. 6. Calculated (points) spectral optical absorption coefficient α is plotted as $(\alpha E)^2$ vs. photon energy (E) for (a) undoped CdO, 0.1%, and 0.6% films; (b) 0.2%, 0.3%, 1.2%, and 2.6% films. The lines in the bandgap absorption region determine the direct bandgaps.

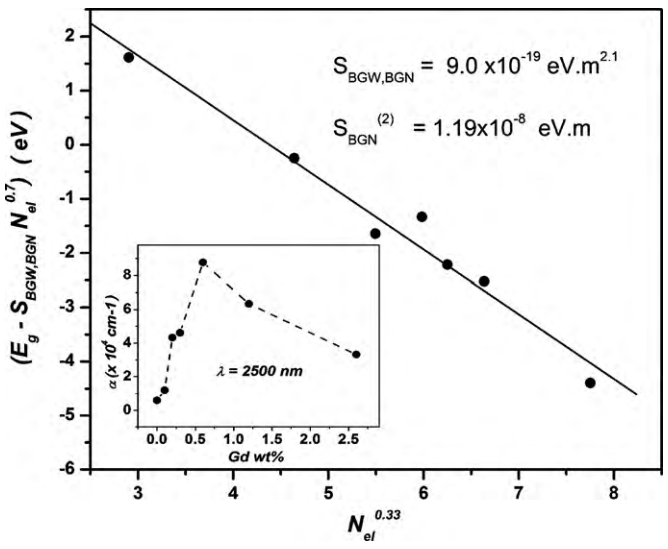

Fig. 7. Dependence of optoelectronic function ($E_g - S_{\mathrm{BGW,BGN}} N_{\mathrm{el}}^{2/3}$) on the carrier concentration $N_{\mathrm{el}}^{1/3}$. The straight line represents the best fit in accordance with Eq. (2). The inset shows the dependence at 2500 nm on the Gd dopant% level.

0.2%Gd narrows its bandgap by about 40%. Such bandgap narrowing (BGN) is associated with an increase in the carrier concentration by around seven times and, thus, it contradicts the Moss–Burstein (B–M) effect [39,40] (i.e. bandgap widening, BGW). This BGN comes as consequence of a change in the nature and strength of the crystalline potential by addition the influence of Gd^{3+} impurity dopant ions including the effect of their 4f-electrons on the crystalline electronic states [41]. So, due to the doping, the band tailing or impurity band becomes broader and finally reaches and merges the bottom of the conduction band causing decrease in the effective optical bandgap E_g [42].

Phenomenologically, it is possible to relate the bandgap variations with the carrier concentration. The BGW (or ΔE_g^{BM}) for parabolic band approximation is given by the following relation [10,11]: $\Delta E_g^{\mathrm{BM}} = S_{\mathrm{BGW}} N_{\mathrm{el}}^{2/3}$, where $S_{\mathrm{BGW}} = (\hbar^2/2\gamma m_e)(3\pi^2)^{2/3}$, $\hbar$ is the Plank's constant and $\gamma = m_{vc}^*/m_e$ is the ratio for of reduced effective mass to free-electron mass, which is equal to 0.274 for undoped CdO [37,38,43]; thus $S_{\mathrm{BGW}}^{\mathrm{th}} = 1.348 \times 10^{-18}\,\mathrm{eV\,m^2}$. The BGN must be taken into the consideration for high density of carriers ($N_{\mathrm{el}} > 10^{19}\,\mathrm{cm^{-3}}$ [44,45]). It consists of two parts. The first part arises due to the electron-impurity interaction leading, for degenerate semiconductor with parabolic band approximation, to the following bandgap shift [43,46]: $\Delta E_{bt} = S_{\mathrm{BGN}}^{(1)} N_{\mathrm{el}}^{2/3}$, where $S_{\mathrm{BGN}}^{(1)} = (1/3) S_{\mathrm{BGW}} = 4.49 \times 10^{-19}\,\mathrm{eV\,m^2}$. The second part of BGN results from the Columbic interaction (C-int) between the carriers, and is given by [47,48] $\Delta E_{\mathrm{C\text{-}int}} = S_{\mathrm{BGN}}^{(2)} N_{\mathrm{el}}^{1/3}$, where $S_{\mathrm{BGN}}^{(2)} = (e/2\pi\varepsilon_0\varepsilon_r)(3/\pi)^{1/3}$, ε_0 is the permittivity of free space, e is the electronic charge, and for the dielectric constant ε_r it is possible to use ε_∞, thus $S_{\mathrm{BGN}}^{(2)} = 2.836 \times 10^{-9}/\varepsilon_r$. Therefore, the total BGN is $\mathrm{BGN} = (S_{\mathrm{BGN}}^{(1)} N_{\mathrm{el}}^{2/3} + S_{\mathrm{BGN}}^{(2)} N_{\mathrm{el}}^{1/3})$ and the overall bandgap shift is

$$\Delta E_g = E_g - E_{g0} = \mathrm{BGW} - \mathrm{BGN} = S_{\mathrm{BGW}} N_{\mathrm{el}}^{2/3} - S_{\mathrm{BGN}}^{(1)} N_{\mathrm{el}}^{2/3} - S_{\mathrm{BGN}}^{(2)} N_{\mathrm{el}}^{1/3} + C_f = S_{\mathrm{BGW,BGN}} N_{\mathrm{el}}^{0.66} - S_{\mathrm{BGN}}^{(2)} N_{\mathrm{el}}^{0.33} + C_f \quad (2)$$

where C_f is the fitting parameter and $S_{\mathrm{BGW,BGN}} = S_{\mathrm{BGW}} - S_{\mathrm{BGN}}^{(1)} = 8.98 \times 10^{-19}\,\mathrm{eV\,m^2}$.

In the present work, a good straight line was obtained by considering the plot of $[E_g - S_{\mathrm{BGW,BGN}} N_{\mathrm{el}}^{0.7}]$ vs. $N_{\mathrm{el}}^{0.33}$, as shown in Fig. 7, with $S_{\mathrm{BGN}}^{(2)} = 1.19 \times 10^{-8}\,\mathrm{eV\,m}$. This value is not close to the theo-

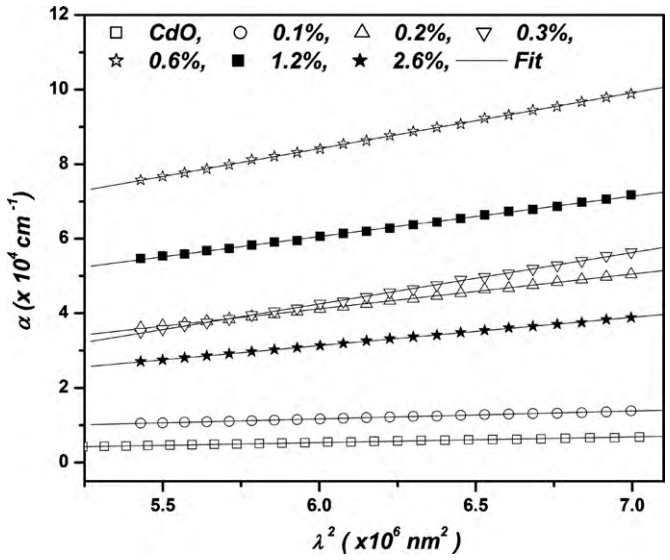

Fig. 8. The dependence of absorption coefficient α on λ^2 in the NIR spectral region for undoped and Gd-doped CdO films.

retical one [1,47] $S^{(2)}_{BGN}(th) = 1.107 \times 10^{-9}$ eV m^2. The used almost empirical relation $\Delta E_g = S_{BGW,BGN} N_{el}^{0.7} - S^{(2)}_{BGN} N_{el}^{0.33} + C_f$ has exponents very close to those in Eq. (2). Furthermore, it is useful to mention here that authors of Refs. [41,49] also proposed pure empirical relations in order to explain their results on BGN. As long as the theoretical basis for the above models is the parabolic band approximation, then it is possible to explain the difference between the theory (Eq. (2)) and the present empirical relation as due to the non-parabolic band effects.

The inset of Fig. 7 demonstrates the dependence of α at 2500 nm (NIR) on Gd% content in the film. This dependence is totally in agreement with the dependence of N_{el} on Gd% content (Fig. 4). This agreement refers to the fact that both dependences related to the same conduction electrons liberated by doping process. This fact was known previously as that the absorption in the NIR spectral region is mainly caused by the free carriers, which can be studied in the framework of classical Drude theory [39]. However, in the NIR spectral region where the reflectivity is almost constant, the absorption coefficient α is related to the wavelength according to [50,51] $\alpha(\lambda) = B_{Op}\lambda^2$ where $B_{Op} = 5.243 \times 10^{-13}(N/\mu)_{Op}(1/n\gamma^2)$ in unit system SI, where n is the refractive index at NIR region $n = 1.6$. Thus by neglecting of the small variations of n in the NIR, a linear α vs. λ^2 relationship should be observed, as shown in Fig. 8. Thus, it is possible to estimate the ratio $(N/\mu)_{op}$ and the results are given in Table 2. The ratios $(N/\mu)_{el}$ (measured electrically) and $(N/\mu)_{Op}$ (measured optically) are different from one another due to different conduction mechanisms (Table 2). Data of Table 2 shows similar trends of the variation of $(N/\mu)_{el}$ and $(N/\mu)_{Op}$.

4. Conclusions

We report on the optical, structural, and dc-electrical properties of Gd-doped CdO films. It was observed that the low doping with Gd^{3+} ions (0.2%) shrinks the bandgap of the host CdO by about 40%. From structural side, 0.6% Gd-doped CdO film has the highest GS and TC. The dc-electrical conduction measurements show that low doping with Gd improves the dc-conduction parameters of CdO, so that the 0.6% Gd-doped CdO film shows increase its mobility by about eight times, conductivity by 150 times, and carrier concentration by 20 times, relative to undoped CdO film. The largest mobility of 66.7 cm^2/V s was observed for 0.2%Gd-doped CdO film. From transparent-conducting-oxide point of view, Gd is sufficiently effective for CdO doping like other metallic dopants such as In, Sn, Sc, and Y.

References

[1] Z. Zhao, D.L. Morel, C.S. Ferekides, Thin Solid Films 413 (2002) 203.
[2] L.M. Su, N. Grote, F. Schmitt, Electron. Lett. 20 (1984) 716.
[3] O. Gomez Daza, A. Arias-Carbajal Readigos, J. Campos, M.T.S. Nair, P.K. Nair, Mod. Phys. Lett. B 17 (2001) 609.
[4] B.J. Lewis, D.C. Paine, Mater. Res. Soc. Bull. 25 (2000) 22.
[5] M. Yan, M. Lane, C.R. Kannewurf, R.P.H. Chang, Appl. Phys. Lett. 78 (2001) 02342.
[6] D.M. Carballeda-Galicia, R. Castanedo-Perez, O. Jimenez-Sandoval, S. Jimenez-Sandoval, G. Torres-Delgado, C.I. Zuniga-Romero, Thin Solid Films 371 (2000) 105.
[7] K.L. Chopra, S. Ranjan Das, Thin Film Solar Cells, Plenum Press, NY, 1993.
[8] Y.S. Choi, C.G. Lee, S.M. Cho, Thin Solid Films 289 (1996) 0153.
[9] R. Kondo, H. Okhimura, Y. Sakai, Jpn. J. Appl. Phys. 10 (1971) 1547.
[10] Powder Diffraction File, Joint Committee for Powder Diffraction Studies (JCPDS) file No. 05-0640.
[11] A.A. Dakhel, Phys. Status Solidi (a) 205 (2008) 2704.
[12] E. Burstein, Phys. Rev. 93 (1954) 632.
[13] T.S. Moss, Proc. Phys. Soc. Lond. B67 (1954) 775.
[14] A.J. Freeman, K.R. Poeppelmeier, T.O. Mason, R.P.H. Chang, T.J. Marks, Mater. Res. Soc. Bull. 25 (2000) 45.
[15] R. Maity, K.K. Chattopadhyay, Sol Energy Mater. Sol. Cells 90 (2006) 597.
[16] S. Shu, Y. Yang, J.E. Medvedova, J.R. Ireland, A.W. Metz, J. Ni, C.R. Kannewurf, A.J. Freeman, T.J. Tobin, J. Am. Chem. Soc. 126 (2004) 13787.
[17] A.A. Dakhel, Thin Solid Films 518 (2010) 1712.
[18] A.A. Dakhel, J. Alloys Compd. 475 (2009) 51.
[19] A.A. Dakhel, Solar Energy 83 (2009) 934.
[20] R.D. Shannon, Acta Crystallogr. A32 (1976) 751.
[21] J.M. Jaklevic, F.S. Goulding, in: H.K. Herglotz, L.S. Birks (Eds.), X-ray Spectrometry, M. Dekker, NY, 1978, p. 50.
[22] T.K. Subramanyam, S. Uthanna, B.S. Naidu, Mater. Lett. 35 (1998) 214.
[23] K.T.R. Reddy, C. Sravani, R.W. Miles, J. Cryst. Growth 184/185 (1998) 1031.
[24] G. Phatak, R. Lai, Thin Solid Films 209 (1992) 240.
[25] K. Tanaka, A. Kunioka, Y. Sakai, Jpn. J. Appl. Phys. 8 (1969) 681.
[26] C.S. Barrett, T.B. Massalski, Structure of Metals, Pergamon, Oxford, 1980, p. 204.
[27] E.F. Kaelble (Ed.), Handbook of X-rays for Diffraction, Emission, Absorption, and Microscopy, McGraw-Hill, New York, 1967, pp. 17–25.
[28] T.L. Chu, S.S. Chu, J. Electron. Mater. 19 (1990) 1003.
[29] K. Gurumurugan, D. Mangalaraj, S.K. Narayandass, J. Electron. Mater. 25 (1996) 765.
[30] A.J. Varkey, A.F. fort, Thin Solid Films 239 (1994) 211.
[31] K.T.R. Reddy, G.M. Shanthini, D. Johnston, R.W. Miles, Thin Solid Films 427 (2003) 397.
[32] X. Li, D.L. Young, H. Moutinho, Y. Yan, C. Narayanswamy, T.A. Gessert, T.J. Coutts, Electrochem. Solid State Lett. 4 (2001) C43.
[33] W.Q. Hong, J. Phys. D: Appl. Phys. 22 (1989) 1384.
[34] J. Rodríguez, M. Gómez, J. Ederth, G.A. Niklasson, C.G. Granqvist, Thin Solid Films 365 (2000) 119.
[35] J. Tauc, In: F. Abeles (Ed.), Optical Properties of Solids, North-Holland Publication, Amsterdam, 1969.
[36] E.A. Davis, N.F. Mott, Philos. Mag. 22 (1970) 903.
[37] K. Kawamura, K. Maekawa, H. Yanagi, M. Hirano, H. Hosono, Thin Solid Films 445 (2003) 182.
[38] N. Ueda, H. Maeda, H. Hosono, H. Kawazoe, J. Appl. Phys. 84 (1998) 6174.
[39] D. Mergel, Z. Qiao, J. Phys. D: Appl. Phys. 35 (2002) 794.
[40] L.K. Dua, A. De, S. Chakraborty, P.K. Biswas, Mater. Charact. 59 (2008) 578.
[41] A.P. Roth, J.B. Webb, D.F. Williams, Phys. Rev. B 25 (1982) 7836.
[42] J.G. Lu, S. Fujita, T. Kawaharamura, H. Nishinaka, Y. Kamada, T. Ohshima, Appl. Phys. Lett. 89 (2006) 262107.
[43] D. Hahn, O. Jaschhinski, H.-H. Wehmann, A. Schlachetzki, J. Electron. Mater. 24 (1995) 1357.
[44] A. Jain, P. Sagar, R.M. Mehra, Solid State Electron. 50 (2006) 1420.
[45] B.E. Sernelius, K.F. Berggren, Z.C. Jin, I. Hamberg, C.G. Granqvist, Phys. Rev. B 37 (1988) 17.
[46] M. Bugajski, W. Lewandowski, J. Appl. Phys. 57 (1985) 521.
[47] P.A. Wolff, Phys. Rev. 126 (1962) 405.
[48] J. Camassel, D. Auvergne, H. Mathieu, J. Appl. Phys. 46 (1975) 2683.
[49] P.E. Schmid, Phys. Rev. B 23 (1981) 5531.
[50] H.L. Hartnagel, A.L. Dawar, A.K. Jain, G. Jagadish, Semiconducting Transparent Thin Films, IOP, Bristol, 1995, p. 226.
[51] A.A. Dakhel, Opt. Mater. 31 (2009) 691.